Developmental Dynamics Special Issue

Short communication (Patterns & Phenotypes)

BMP4 regulates asymmetric Pkd2 distribution in mouse nodal immotile cilia and ciliary mechanosensing required for left–right determination

Takanobu A. Katoh[1,2,*], Tim Lange[2], Yoshiro Nakajima[3], Kenta Yashiro[3], Yasushi Okada[1,4,5], Hiroshi Hamada[2]

[1] Department of Cell Biology, Graduate School of Medicine, The University of Tokyo, Tokyo 113-0033, Japan

[2] Laboratory for Organismal Patterning, RIKEN Center for Biosystems Dynamics Research, Kobe 650-0047, Japan

[3]Division of Anatomy and Developmental Biology, Department of Anatomy, Kyoto Prefectural University of Medicine, Kyoto 602-8566, Japan

[4]Laboratory for Cell Polarity Regulation, RIKEN Center for Biosystems Dynamics Research, Suita, Osaka, Japan

[5]Department of Physics, Universal Biology Institute and International Research Center for Neurointelligence, The University of Tokyo, Hongo, Tokyo, Japan

***Corresponding Author**

Takanobu A. Katoh

Current affiliation: Department of Cell Biology, Graduate School of Medicine, The University of Tokyo, Tokyo 113-0033, Japan

Tel: +81-3-5841-3676

E-mail: takanobu.a.katoh@gmail.com

Running Title:

BMP4 regulates cilia Pkd2 distribution

Keywords:

Left–right symmetry breaking
Mouse nodal immotile cilia
Pkd2
STED microscopy
Optical tweezers
Mechanobiology

Grant Sponsor

This study was supported by the FOREST Program (grant no. JPMJFR224N) of the Japan Science and Technology Agency (JST), Grant-in-Aid (grant no. 21K15096, 24K18107, and 24H01270) from the Japan Society for the Promotion of Science (JSPS), RIKEN Special Postdoctoral Researcher Program, The University of Tokyo Excellent Young Researcher Program, Ultrastructure Research Fund from The Japanese Society of Microscopy to T.A.K.; by a grant from the Japan Society for the Promotion of Science (no. 17H01435) to H.H.; by JSPS grants 19H05794, 19H05795 and 22H04926; JST grants JPMJMS2025-14, JPMJCR20E2 to Y.O. This work was supported in part by the University of Tokyo Research Internship Program (UTRIP) 2023 to Y.O.

Conflict of Interest Disclosure

The authors declare no conflicts of interest.

Abstract

Background

Mouse nodal immotile cilia mechanically sense the bending direction for left–right (L–R) determination and activate the left-side-specific signaling cascade, leading to increased *Nodal* activity. Asymmetric distribution of Pkd2, a crucial channel for L-R determination, on immotile cilia has been reported recently. However, the causal relationship between the asymmetric Pkd2 distribution and direction-dependent flow sensing is not well understood. Furthermore, the underlying molecular mechanism directing this asymmetric Pkd2 distribution remains unclear.

Results

The effects of several recombinant proteins and inhibitors on the Pkd2 distribution were analyzed using super-resolution microscopy. Notably, bone morphogenetic protein 4 (BMP4) affected the Pkd2 distribution. Additionally, three-dimensional manipulation of nodal immotile cilia using optical tweezers revealed that excess BMP4 caused defects in the mechanosensing ability of the cilia.

Conclusions

Experimental data together with model calculations suggest that BMP4 regulates the asymmetric distribution of Pkd2 in nodal immotile cilia, thereby affecting the ability of these cilia to sense the bending direction for L–R determination. This study, for the first time, provides insight into the relationship between the asymmetric protein distribution in cilia and their function.

1 Introduction

Establishment of left–right asymmetry in vertebrate embryos first occurs in the left–right organizer, known as the node in mice.[1] The node is a small cavity located at the midline and is composed of two types of ciliated cells: pit cells in the central region of the node that possess motile cilia[2] and generate the leftward nodal flow responsible for establishing left–right determination[3] and crown cells in the

peripheral region of the node that possess immotile (primary) cilia.[4] Leftward nodal flow mechanically activates the Pkd2 channel localized on immotile cilia,[5,6] leading to an increase in the frequency of calcium transients only on the left side of the cilia and cytoplasm.[7,8] Particularly, leftward nodal flow causes passive mechanical bending of immotile cilia in an asymmetrical manner, wherein the left- and right-side cilia show ventral and dorsal bending, respectively.[5] A previous experiment involving the artificial manipulation of immotile cilia in three dimensions using optical tweezers revealed that nodal immotile cilia preferentially respond to ventral bending,[5] in the same bending direction applied to left-side cilia by leftward nodal flow. Therefore, only the left-side immotile cilia are activated by left-ward nodal flow. Activation of left-side immotile cilia induces degradation of *Dand5* mRNA, whose protein acts as an antagonist to *Nodal* and activates left-side-specific *Nodal* activity in crown cells.[9]

The Pkd2 channel was recently reported to exhibit asymmetric localization on immotile cilia, which may play a crucial role in the initial step of left–right symmetry breaking. Precise measurement of the membrane strain distribution during ventral bending induced by nodal flow suggested a relationship between the preferential response to ventral bending and the asymmetric Pkd2 distribution. Notably, passive ventral bending induces an increase in strain on the dorsal side of the cilia, where Pkd2 is preferentially localized.[5] Therefore, the nodal immotile cilia may specifically sense dorsal bending. Dorsal localization of Pkd2 on cilia may be associated with the dorsoventral (D–V) and/or midline–lateral polarity. The asymmetric distribution of flagellar proteins, such as Hv1,[10] has been reported in human sperm; however, the mechanism by which the asymmetric Pkd2 distribution is generated in immotile cilia remains unknown.

Pit cells, located at the center of the node, exhibit planar cell polarity along the anterior–posterior axis,[11,12] and play a role in generating leftward nodal flow.[3,13–15] Although cell polarity along the midline to lateral direction has not been evaluated, some factors exhibit a gradient from the midline to lateral regions. These factors may be involved in regulating the asymmetric distribution of Pkd2. For instance, Noggin and Chordin, an antagonists of bone morphogenetic protein 4 (BMP4),[16] are expressed in the node and notochord, whereas BMP4 is expressed in the lateral plate mesoderm (LPM) from the emergence to disappearance of the node. We previously reported that exogenous BMP2 does not significantly affect Pkd2 localization on immotile cilia,[5] however, BMP4 is expressed in the LPM. The interaction of Noggin and Chordin with BMP4 may generate a concentration gradient. Another potential candidate is the sonic hedgehog (SHH), which is expressed in the node and notochord.[17] SHH, an extracellular protein involved in numerous signaling pathways, may generate a concentration gradient from the node to LPM. Notch2 is expressed near the node, whereas delta-like 1 is expressed in the area surrounding the node.[18] These two genes regulate hair-bundle polarity in lateral-line hair cells.[19,20] Hence, they may contribute to the establishment of polarity along

the midline to lateral direction in crown cells. Furthermore, fibroblast growth factor 8 (FGF8) is expressed in the primitive streak of E7.5 embryos[21] and may affect D–V polarity. We predicted that these factors establish the concentration gradient and/or polarity responsible for the asymmetric distribution of Pkd2.

Additionally, the scaffold protein in cilia may be involved in generating and maintaining the asymmetric distribution of Pkd2. Notably, the Pkd2-mastigoneme complex forms a linear array in *Chlamydomonas.*[22–24] Although mastigonemes have not been reported in nodal cilia, Pkd2 may require other binding partners and/or scaffolds, such as Inversin. *Inversin* mutant mice exhibit *situs inversus*,[25] and Inversin, with its compartment composed of a fibrilloid structure, may function as a scaffold.[26] In this study, we evaluated the contribution of these factors to the asymmetric distribution of Pkd2. We also examined the relationship between the mechanosensory ability and organized distribution of Pkd2 in mouse nodal immotile cilia.

2 Results

2.1 Excess BMP4 disrupts correctly organized Pkd2 distribution in nodal immotile cilia

We examined whether the candidate factors BMP4, Noggin, Chordin, SHH signaling, Notch signaling, and FGF8 are responsible for the asymmetric distribution of Pkd2. The asymmetric distribution of Pkd2 was evaluated using confocal microscopy with an Airyscan detector after treatment with the candidates. Pkd2 in the nodal immotile cilia was observed using the *NDE2–hsp–Pkd2–Venus* transgene,[6] which is driven by the nodal-specific enhancer (NDE) derived from the mouse *Nodal* gene (Figure 1A). Embryos harboring the transgene were cultured from the late bud (LB) stage, just before the beginning of node formation, to the 0–2 somite stages (ss), which is the period when symmetry breaking occurs, with or without the reagent of interest (Figure 1A). The distance along the *z*-axis between the center of Pkd2 localization and the axoneme, which represents the localization of Pkd2 protein in a cilium, was analyzed using Gaussian fitting (Figure 1B).

First, we examined the effect of BMP4 signaling by supplementing the medium with recombinant BMP4 or its antagonists, Noggin and Chordin. In embryos treated with 1 μg/mL recombinant BMP4, the distance between the center of cilia and location of Pkd2 in immotile cilia was apparently more polarized (133 ± 122 nm; mean ± standard deviation) toward the dorsal side compared with that in the control (Figure 1C). In contrast, Pkd2 localization did not significantly differ between the Noggin-treated and control embryos or between the Noggin and Chordin double-treated and control embryos (Figure 1D). We next evaluated the effects of SHH signaling in mutant

embryos lacking *Smo*,[27] which encodes a G protein-coupled receptor that plays a crucial role in the Hedgehog signaling pathway. Pkd2 localization did not significantly differ between *Smo*$^{-/-}$ mutant and control embryos (Figure 1E, F). Finally, we investigated the involvement of Notch signaling by supplementing the medium with *N*-[*N*-(3, 5-difluorophenacetyl)-l-alanyl]-*S*-phenylglycine *t*-butyl ester (DAPT), a γ-secretase inhibitor. No significant difference was observed in Pkd2 localization between DAPT-treated and control embryos (Figure 1G, H). The effect of FGF signaling was examined by supplementing the medium with recombinant FGF8 or SU5402 (inhibitor of the tyrosine kinase activity of FGF and vascular endothelial growth factor receptors). These treatments did not significantly affect Pkd2 localization (Figure 1I, J).

The results, derived from Airyscan images, suggest that an excessive amount of BMP4 influences the proper distribution of Pkd2 in immotile cilia, with no involvement of other signaling factors. To confirm the effects of BMP4, Pkd2 localization in immotile cilia was examined using 3D-stimulated emission depletion (STED) microscopy, which achieved a resolution of <100 nm in the *x*, *y*, and *z* directions.[28] We determined the angular distribution of Pkd2::Venus protein on the transverse plane of the axoneme by measuring the Venus intensity and angle from the center of gravity of acetylated tubulin (Figure 2A).[29] Analysis of the STED images revealed that cilia in BMP4-treated embryos exhibited a significantly biased Pkd2 distribution toward the dorsal side with a D/(D + V) ratio of 0.65 ± 0.14 (n = 40; Figure 2B, C) compared with that in the control embryos with a ratio of 0.54 ± 0.12, as previously reported.[5] In contrast, cilia on Noggin-treated embryos showed an asymmetric distribution with a D/(D + V) ratio of 0.55 ± 0.09 (n = 36), which was similar to that in the control (Figure 2B, D).

To assess the association between the scaffold protein Inversin in cilia and asymmetric distribution of Pkd2, we used *Inv/Inv* mutant mice. The localization of Pkd2 in immotile cilia was evaluated using STED microscopy, employing the Pkd2 antibody rather than the *Pkd2–Venus* transgene. Cilia on *Inv/Inv* embryos exhibited an asymmetric distribution with a D/(D + V) ratio of 0.57 ± 0.10 (n = 64), which was similar to that in control embryos with a ratio of 0.54 ± 0.14, as previously reported[5] (Figure 2E). These results indicate that excess BMP4 disrupts the correct distribution pattern of Pkd2, inducing a more polarized distribution toward the dorsal side of nodal immotile cilia.

2.2 Model calculation supports that the BMP4 concentration gradient is involved in an asymmetric Pkd2 distribution

We conducted model calculations to determine the effect of BMP4 on Pkd2. Initially, we estimated the concentration gradient of BMP4 in the node of both wild-type (WT) embryos and

BMP4-treated embryos (Figure 3A, B). In the WT embryo model, BMP4 was secreted from the left LPM. We set the BMP4 concentration of the LPM as 1 nM; the molecules diffused with a diffusion constant of 3 $\mu m^2/s$ (Table 1). Nodal immotile cilia were located 120 µm away from the LPM. Despite considering internalization and non-specific degradation, measured as a clearance rate of 8.9 $\times$ $10^{-5}/s$[30] (Table 1), some secreted BMP4 reached the node and generated a concentration gradient (Figure 3C). The estimated BMP4 concentration gradient at the nodal immotile cilia was approximately 0.001 nM/µm in WT (Figure 3D). In contrast, in the model under BMP4-treated conditions, the node depth was 12 µm, with the immotile cilia 6 µm from the bottom of the node. Considering the BMP4 clearance on the node surface (Table 1), a BMP4 concentration gradient was expected to from along the node depth (Figure 3E). The estimated BMP4 concentration gradient at the nodal immotile cilia was approximately 5.2 nM/µm under the BMP4-treated condition (Figure 3F). Based on the parameters derived from measurements in previous reports, the BMP4 concentration gradient at the nodal immotile cilia was significantly increased under the BMP4-treated condition.

The relationship between the BMP4 concentration gradient and regulation of the Pkd2 asymmetric distribution remains unknown. A plausible hypothesis is that the BMP4 concentration influences the Pkd2 distribution by biasing the diffusion of Pkd2 in response to the BMP4 concentration gradient. In this hypothetical model, when the BMP4 concentration decreased toward the center (bottom) of the node, Pkd2 molecules exhibited biased diffusion, showing preferential movement toward the dorsal side. We chose '*S*' (sensitivity of BMP4 concentration gradient for regulation of Pkd2 distribution; Table 1) as a model parameter to match the experimental values (see Methods). Through this parameter adjustment, the model successfully reproduced the Pkd2 asymmetric distribution observed in the experimental data (Figure 3D, F). These models indicate that the BMP4 concentration gradient influences the generation of the asymmetric Pkd2 distribution (Figure 3A, B).

2.3 Excess BMP4 disrupts the calcium response in crown cells triggered by mechanical stimuli to the cilium

To examine the relationship between the asymmetric Pkd2 distribution and its ability to sense the bending direction of immotile cilia, we used optical tweezers to manipulate individual immotile cilia and simultaneously measure the calcium response in the cytoplasm of crown cells.[5] Briefly, *iv/iv* embryos harboring the *NDE4–hsp–5HT$_6$–GCaMP6–2A–5HT$_6$–mCherry*[5,7] and *NDE4–hsp–GCaMP6*[5] transgenes were cultured from the LB to 0–2 ss in the presence of recombinant BMP4 or Noggin protein (Figure 4A). The frequency of calcium transients in the cytoplasm was assessed while applying dorsal and ventral bending of the cilium using a 3.5-µm-diameter bead trapped using optical

tweezers[5,29,31] (Figure 4A). Immotile cilia in the left–right organizer of mouse[5] and zebrafish[32] embryos function as mechanosensors. Furthermore, in mouse embryos, these immotile cilia preferentially sense ventral bending.[5] We postulated that the asymmetric distribution of Pkd2 is associated with this directional sensing of bending.

In BMP4-treated embryos, crown cells exhibited intrinsic calcium oscillations, as previously reported[5,7,8]; however, the calcium frequency under dorsal or ventral bending was not significantly increased compared with that before applying mechanical stimuli (Figure 4B). This result indicates that nodal immotile cilia did not respond to mechanical stimuli under treatment with excess BMP4. In contrast, in Noggin-treated embryos, the calcium frequency was significantly increased under ventral bending compared with that under dorsal bending or before applying mechanical stimuli (Figure 4C), similarly to in the WT embryos, as previously reported.[5] Therefore, Noggin-treated cilia retained the ability to sense the bending direction, whereas BMP4-treated cilia lost their mechanosensing ability. Hence, correctly organized asymmetric distribution of Pkd2 in cilia may be crucial for sensing the bending direction as well as for mechanosensing ability.

3 Discussion

BMP4 functions in left–right determination within the context of Nodal expression in the LPM. When left-sided-specific Nodal activation occurs at the node, the signal is transmitted to the LPM.[33] In the LPM, a self-enhancement and lateral-inhibition system involving Nodal and Lefty maintains robust Nodal expression.[34] As BMP signaling represses Nodal expression in the LPM, the antagonism of BMP by Noggin and Chordin in the left LPM relieves the repressive effects of BMP on Nodal expression. Therefore, the asymmetric BMP signal distribution is involved in maintaining left–right asymmetric Nodal expression in the LPM.[16] In this study, we observed an additional role for BMP4 in left–right determination. Notably, a specific concentration gradient of BMP4 is necessary to generate a correctly organized asymmetric distribution of Pkd2 on cilia, thus affecting their mechanosensing ability. The precise mechanism underlying regulation of the Pkd2 distribution by the BMP4 concentration remains unknown; however, cilia or the apical surface of crown cells may sense the BMP4 concentration gradient along the D–V axis, which would place Pkd2 molecules away from the higher BMP4 concentration (Figure 3A, B), bringing more Pkd2 molecules to the dorsal side. In contrast, Inversin, the scaffold protein in cilia, is not involved in generating the asymmetric Pkd2 distribution.

The model calculation explained why Pkd2 distribution was more polarized toward the dorsal side in the presence of excess BMP4. However, the biophysical mechanism underlying detection of the BMP4 concentration gradient, particularly sensing of the shallow gradient of 0.001 nM/μm in the WT embryos, remains unknown. Based on studies of the physics of chemoreception in

microorganisms,[35] sensing through the cell surface or a multicellular system coupled with sufficient observation (integral) time is a more plausible mechanism than a simple receptor-based sensing system within cilia. Notably, node emergence and ciliogenesis occur during the mid-streak to late streak stages.[36] In contrast, BMP4 expression begins in the extra-embryonic mesoderm before node emergence and later detected in the posterior primitive streak and LPM at embryonic day 7.5[16,37,38]. Based on these reports, the BMP4 concentration gradient may emerge prior to node formation. Subsequently, during ciliogenesis and by utilizing this BMP4 concentration gradient, Pkd2 may gradually be asymmetrically distributed over time.

The molecular pathway responsible for regulating the Pkd2 distribution via the BMP4 concentration gradient requires further analysis. Particularly, the reasons why Noggin and Chordin did not affect the Pkd2 distribution remain unclear. Dand5, which is expressed in the crown cells and functions as an antagonist of BMP4, may lead to these effects. However, to establish a robust concentration gradient along the midline–lateral direction, BMP4 should antagonize a molecule expressed in the center of the node, such as those found in pit cells. Another possibility is the compensatory effect of BMPs, as BMPs exhibit considerable overlap in receptor-binding specificity. For instance, both BMP4 and BMP6 bind to BMP receptor-II.[39] Notably, Noggin showed a stronger inhibitory effect on BMP4 than on BMP6 in receptor binding[40]. Following Noggin treatment, other BMPs, such as BMP6, may compensate for the function of BMP4. BMP6 is expressed in the yolk sac endoderm and anterior cardiogenic mesoderm on embryonic day 7.0 in mouse embryos,[41] suggesting that is plays a role in generating concentration gradients from the lateral side of the embryo to the node. Pkd2 is trafficked to the cilia through its C-terminus, where it interacts with PKD1. Notably, Pkd1 harbors a cilia-targeting sequence at its C-terminus[42]. However, the precise mechanism by which the BMP4 concentration gradient regulates the Pkd2 distribution remains unclear. Certain molecules capable of sensing BMP4 may be involved in regulating the asymmetric Pkd2 distribution. To identify proteins that may interact with BMP4, we conducted a search using BioGRID,[43] focusing on ciliary proteins,[44–46] and identified the following nine candidates: CACL, MAP4, RPL4, RPL7, RPL9, RPL12, RPL18, RPL21, and SYNCRIP. SUFU was excluded from the list because *Smo* was not involved in regulating the Pkd2 distribution (Figure 1F). These nine candidates may be involved in regulating the Pkd2 distribution. Furthermore, BMP receptors are localized at the base of osteoblast cilia.[47] Although the expression of these candidates in nodal immotile cilia has not been evaluated, they may be involved in regulating the asymmetric distribution of Pkd2.

Our data demonstrate that an organized asymmetric Pkd2 distribution is necessary for the mechanosensing ability of nodal immotile cilia. However, the exact mechanism of bending-direction sensing using dorsally localized Pkd2 remains unknown. We induced excessive dorsal localization of Pkd2 via BMP4 treatment. We hypothesized that the cilia exhibit an exaggerated response to ventral bending, based on our previous study, as excessive dorsal localization of Pkd2 may be more sensitive to the increase in membrane tension on the dorsal side of the cilia caused by ventral bending.

However, we found that the cilia lost their mechanosensing ability rather than exhibiting an exaggerated response to ventral bending. The reason for this loss of mechanosensing ability in cilia under BMP4 treatment requires further analysis. However, this may be attributed to the loss of the mechanosensing function of Pkd2. Pkd2 functions by forming a heterocomplex with Pkd1l1 in the nodal immotile cilia.[48,49] Excessively polarized localization of Pkd2 may prevent the correct formation of a complex with Pkd1l1 in the cilia. Considering the report on the Pkd2–mastigoneme complex in *Chlamydomonas*,[22–24] Pkd2 may require other binding partners and/or scaffolds, such as Inversin,[25,26] for its mechanosensing function, although Inversin was not involved in generating the asymmetric Pkd2 distribution (Figure 2E). Notably, excessive BMP4 may affect these interactions. Another possibility is that excessive BMP4 may disrupt signal transduction from the cilia to the cytoplasm. We previously reported that calcium transients in cilia trigger calcium release from the endoplasmic reticulum, which is abundant in the apical region of crown cells, in an IP3 receptor-dependent manner.[7] This cascade then activates *Dand5* mRNA degradation, ultimately establishing left–right asymmetry[7,9]. Although reports on the effect of BMP4 on this cascade remain lacking, BMP4 may disrupt signal transduction through this pathway. Further studies are needed to understand the molecular mechanism underlying the establishment of the organized polarized Pkd2 distribution based on the BMP4 concentration gradient.

4 Experimental Procedures

4.1 Mice and transgenes

Smo$^{+/-}$ mice (strain B6(D2)-Smo<Rgsc2073>) were obtained from the Riken Bioresource Center (Ibaraki, Japan). Transgenic mouse lines harboring *NDE2–hsp–Pkd2–Venus*[6], *NDE4–hsp–GCaMP6–pA*[5], and *NDE4–hsp–5HT$_6$–GCaMP6–2A–5HT$_6$–mCherry*[7] were previously reported. *Inv/Inv* mutant mice were previously reported[25]. All animal experiments were approved by the Institutional Animal Care and Use Committee of the RIKEN Kobe Branch and Committee for Animal Research of Kyoto Prefectural University of Medicine.

4.2 Embryo culture

Mouse embryos were collected on embryonic day 7.5 in HEPES-buffered Dulbecco's modified Eagle's medium (DMEM, pH 7.2). Embryos at the LB stage were selected and cultured using the roller culture method at 5% CO_2 and 37 °C in 50-mL tubes containing DMEM supplemented with 75% rat serum. Agents were added to the medium at final concentrations of 1 μg/mL for BMP4

319 treatment (314-BP; R&D Systems, Minneapolis, MN, USA), 1% v/v of 4 mM HCl containing 0.1%
320 bovine serum albumin (BSA; A3311; Sigma-Aldrich, St. Louis, MO, USA) as the control of BMP4
321 treatment, 1 μg/mL for Noggin treatment (1967-NG; R&D Systems), 1% v/v of phosphate-buffered
322 saline (PBS) containing 0.1% BSA as the control of Noggin treatment, 1 μg/mL Noggin and 1 μg/mL
323 Chordin as double treatment (758-CN; R&D Systems), 2% v/v of PBS containing 0.1% BSA as the
324 control Noggin and Chordin double treatment, 200 μM for DAPT (AG-CR1-0016; AdipoGen, San
325 Diego, CA, USA), 25 μM for SU5402 (CS-0200; ChemScene, Monmouth Junction, NJ, USA),
326 0.4325% dimethyl sulfoxide (276855; Sigma-Aldrich) as the control of DAPT treatment or SU5402
327 treatment, and 1 μg/mL for FGF-8b (423-F8; R&D Systems), 0.5% v/v of PBS containing 0.1% BSA
328 as the control of FGF-8b treatment.
329

330 4.3 Analysis of Pkd2 localization in immotile cilia

331 Pkd2 localization in immotile cilia was analyzed as previously described.[5,29] After roller culture, the
332 embryos were washed with PBS. Immunostaining was performed as previously described.[5,29] Anti-
333 acetylated tubulin (1:200 dilution; T6793; Sigma-Aldrich) and anti-green fluorescent protein (1:200
334 dilution; ab13970; Abcam, Cambridge, UK) primary antibodies were used. The pair of secondary
335 antibodies used were anti-chick and anti-mouse conjugated either with AlexaFluor Plus 488 (1:200
336 dilution; A32931; Invitrogen, Carlsbad, CA, USA) and AlexaFluor Plus 555 (1:200 dilution; A32727;
337 Invitrogen) for Airyscan observation or STAR ORANGE (1:200 dilution; anti-chick; Abberior,
338 Göttingen, Germany) and STAR RED (1:200 dilution; anti-mouse; Abberior) for STED observation.
339 The nodes were observed using a Zeiss LSM 880 (Oberkochen, Germany) with an Airyscan
340 confocal microscope equipped with 100× (alpha-Plan-APOCHROMAT 100 Oil for SR 1.46 N.A.)
341 lenses. For accurate measurement, the treatment and control embryos were alternately measured with
342 in the same experiment set. 3D images were recorded with 2 × 2 tiling and depth along the *z*-axis of
343 168 nm. After Airyscan processing, the distance along the *z*-axis between the centers of the red and
344 green channels was measured via Gaussian fitting with a fitting error of $\sigma < 20$ nm, as previously
345 described.[5] 3D-STED imaging was performed using an Infinity instrument (Abberior) equipped with a
346 60× lens (UPLXAPO60XO 1.4 N.A.; Olympus, Tokyo, Japan) as previously described.[5,29] Image
347 processing and analysis of the angular distribution of the intensity of Pkd2 signals were conducted as
348 previously described.[5,29] For *Inv/Inv* embryos, we used a Pkd2 antibody (1:50 dilution; sc-28331,
349 Santa Cruz Biotechnology, Dallas, TX, USA) for immunostaining, as previously reported.[5]
350

4.4 Manipulation of cilia using optical tweezers and analysis of calcium transients

A distal portion of each embryo including the node after roller culture with agents was excised, placed in a chamber consisting of a glass slide fitted with a thick silicone rubber spacer (thickness: 400 μm), covered with a coverslip (No.1S; Matsunami), and incubated at 5% CO_2 and 37 °C in FluoroBrite DMEM (A1896701; Thermo Fisher Scientific, Waltham, MA, USA) supplemented with 75% rat serum and agents. The experiment using optical tweezers[50] was performed using an IX83/CSU-W1 microscope equipped with a 60× lens (UPLSAPO 60XW 1.2 N.A.; Olympus), single-mode fiber laser (wavelength of 1064 nm; YLR-5-1064-LP-SF; IPG Photonics, Novi, MI, USA), and filter set (ZT1064rdc-sp-UF3, Chroma Technology, Bellows Falls, VT, USA and SIX870; Asahi, Tokyo, Japan) as previously described.[5,29]

4.5 Model and numerical simulations

Diffusion of BMP4 was calculated using the following equation:

$$\frac{\partial B}{\partial t} = D_B \frac{\partial^2}{\partial x^2} B - \lambda B$$

where B, λ, and D_B represent the concentration, degradation constant, and diffusion constant of BMP4, respectively. As values for λ and D_B, we used reported values obtained for BMP2b in zebrafish embryos.[30] Although the precise concentration of B in the LPM of WT embryos was unknown, it was estimated to be approximately the order of 1 nM. The values of each parameter are listed in Table 1. The geometric configurations of the models are illustrated in Figure 3C for WT embryos and Figure 3E for BMP4-treated embryos. In the model, the concentration of B at $x = 0$ was fixed at 1 nM for the WT and 30 μM (1 μg/mL) for the BMP4-treated condition. The initial concentration of BMP4 was 0, except where at $x = 0$. The boundary conditions were defined by the no-flux condition at the center of the node (L) for the WT and at the bottom of the node (L) for the BMP4-treated condition: $\nabla B|_{x=L} = 0$. For numerical simulations of the model, we used the Crank–Nicolson scheme with 751 grids for WT and 61 grids for BMP4-treated condition (grid width, 200 nm) and a constant time step of Δt = 0.001s.

The distribution of Pkd2 molecules in the cilium was modeled by simulating the diffusion of individual Pkd2 molecules along the *x*-axis, representing the dorsoventral (transverse) axis of the cilium, with the diffusion constant D_{Pkd}. The cilium was divided into 10 steps (width of each step, 0.1, corresponding to 20 nm) along the *x*-axis, and each Pkd2 molecule was moved with the following probabilities:

$$Step\ size = \begin{cases} +0.1 \cdots Probability: p - p \times S \times \partial B(t)/\partial x|_{x=location\ of\ cilium} \\ -0.1 \cdots Probability: p + p \times S \times \partial B(t)/\partial x|_{x=location\ of\ cilium} \\ 0 \cdots Probability: 1 - 2p \end{cases}$$

where $p = \Delta t \times D_{Pkd}/(step\ size)^2$ and S is the sensitivity of BMP4 concentration gradient for Pkd2 distribution regulation. When the BMP4 concentration gradient ($\partial B(t)/\partial x$) was 0, indicating the absence of a BMP4 concentration gradient, Pkd2 molecules exhibited free diffusion. In contrast, when $\partial B(t)/\partial x$ was a negative value, indicating a decrease in the BMP4 concentration toward the center (bottom) of the node, Pkd2 molecules showed biased diffusion toward the dorsal side depending on the parameter, *S*. The diffusion constant of Pkd2 within cilia was approximated using the value of PTCH1.[51] The parameter *S* was selected to ensure that the model replicated the observed asymmetric Pkd2 distribution observed via STED microscopy. The boundary conditions were defined by the reflective conditions at both the dorsal and ventral edges of the cilium. For numerical simulations, 100 Pkd2 molecules were initially located at the center of the cilia and then diffused according to the model, and the positions of these molecules during 4500–5000 s (for WT; Figure 3D) and 3100–3600 s (for the BMP4-treated condition; Figure 3F) were plotted as the D/(D + V) ratio.

4.6 Statistical analysis

Statistical analysis and graph preparation were performed using IgorPro 8 (WaveMetrics, Portland, OR, USA). Three-dimensional reconstructed images were generated using Imaris software (Oxford Instruments, Oxford, UK). All statistical tests are described in the figure legends. $P < 0.05$ was considered statistically significant.

Acknowledgments

We would like to thank X. Sai, S. Hiver, Y. Ikawa, and H. Nishimura for providing assistance with the mouse embryo experiments, H.Y. Liu and S. Orii for help with STED image analysis; and T. Furuya for secretarial assistance. Additionally, we would like to thank K. Kawaguchi and members of his laboratory, as well as the members of the Okada laboratory, for their helpful discussion.

References

1. Hamada H. Molecular and cellular basis of left–right asymmetry in vertebrates. *Proc Jpn Acad Ser B*. 2020;96(7):273-296. https://doi.org/10.2183/pjab.96.021
2. Nonaka S, Tanaka Y, Okada Y, et al. Randomization of Left–Right Asymmetry due to Loss of Nodal Cilia Generating Leftward Flow of Extraembryonic Fluid in Mice Lacking KIF3B Motor Protein. *Cell*. 1998;95(6):829-837. https://doi.org/10.1016/S0092-8674(00)81705-5
3. Okada Y, Takeda S, Tanaka Y, Belmonte JCI, Hirokawa N. Mechanism of Nodal Flow: A Conserved Symmetry Breaking Event in Left-Right Axis Determination. *Cell*. 2005;121(4):633-644. https://doi.org/10.1016/j.cell.2005.04.008
4. McGrath J, Somlo S, Makova S, Tian X, Brueckner M. Two Populations of Node Monocilia Initiate Left-Right Asymmetry in the Mouse. *Cell*. 2003;114(1):61-73. https://doi.org/10.1016/S0092-8674(03)00511-7
5. Katoh TA, Omori T, Mizuno K, et al. Immotile cilia mechanically sense the direction of fluid flow for left-right determination. *Science*. 2023;379(6627):66-71. https://doi.org/10.1126/science.abq8148
6. Yoshiba S, Shiratori H, Kuo IY, et al. Cilia at the Node of Mouse Embryos Sense Fluid Flow for Left-Right Determination via Pkd2. *Science*. 2012;338(6104):226-231. https://doi.org/10.1126/science.1222538
7. Mizuno K, Shiozawa K, Katoh TA, et al. Role of Ca^{2+} transients at the node of the mouse embryo in breaking of left-right symmetry. *Sci Adv*. 2020;6(30):eaba1195. https://doi.org/10.1126/sciadv.aba1195
8. Takao D, Nemoto T, Abe T, et al. Asymmetric distribution of dynamic calcium signals in the node of mouse embryo during left–right axis formation. *Dev Biol*. 2013;376(1):23-30. https://doi.org/10.1016/j.ydbio.2013.01.018
9. Minegishi K, Rothé B, Komatsu KR, et al. Fluid flow-induced left-right asymmetric decay of Dand5 mRNA in the mouse embryo requires a Bicc1-Ccr4 RNA degradation complex. *Nat Commun*. 2021;12(1):4071. https://doi.org/10.1038/s41467-021-24295-2
10. Miller MR, Kenny SJ, Mannowetz N, et al. Asymmetrically Positioned Flagellar Control Units Regulate Human Sperm Rotation. *Cell Rep*. 2018;24(10):2606-2613. https://doi.org/10.1016/j.celrep.2018.08.016
11. Hashimoto M, Shinohara K, Wang J, et al. Planar polarization of node cells determines the rotational axis of node cilia. *Nat Cell Biol*. 2010;12(2):170-176. https://doi.org/10.1038/ncb2020
12. Song H, Hu J, Chen W, et al. Planar cell polarity breaks bilateral symmetry by controlling ciliary positioning. *Nature*. 2010;466(7304):378-382. https://doi.org/10.1038/nature09129
13. Cartwright JHE, Piro O, Tuval I. Fluid-dynamical basis of the embryonic development of left-right asymmetry in vertebrates. *Proc Natl Acad Sci*. 2004;101(19):7234-7239. https://doi.org/10.1073/pnas.0402001101
14. Nonaka S, Yoshiba S, Watanabe D, et al. De Novo Formation of Left–Right Asymmetry by Posterior Tilt of Nodal Cilia. *PLOS Biol*. 2005;3(8):e268. https://doi.org/10.1371/journal.pbio.0030268

15. Sai X, Ikawa Y, Nishimura H, et al. Planar cell polarity-dependent asymmetric organization of microtubules for polarized positioning of the basal body in node cells. *Development*. 2022;149(9):dev200315. https://doi.org/10.1242/dev.200315
16. Mine N, Anderson RM, Klingensmith J. BMP antagonism is required in both the node and lateral plate mesoderm for mammalian left-right axis establishment. *Development*. 2008;135(14):2425-2434. https://doi.org/10.1242/dev.018986
17. Tsukui T, Capdevila J, Tamura K, et al. Multiple left-right asymmetry defects in Shh−/− mutant mice unveil a convergence of the Shh and retinoic acid pathways in the control of Lefty-1. *Proc Natl Acad Sci*. 1999;96(20):11376-11381. https://doi.org/10.1073/pnas.96.20.11376
18. Krebs LT, Iwai N, Nonaka S, et al. Notch signaling regulates left–right asymmetry determination by inducing Nodal expression. *Genes Dev*. 2003;17(10):1207-1212. https://doi.org/10.1101/gad.1084703
19. Jacobo A, Dasgupta A, Erzberger A, Siletti K, Hudspeth AJ. Notch-Mediated Determination of Hair-Bundle Polarity in Mechanosensory Hair Cells of the Zebrafish Lateral Line. *Curr Biol*. 2019;29(21):3579-3587.e7. https://doi.org/10.1016/j.cub.2019.08.060
20. Jiang T, Kindt K, Wu DK. Transcription factor Emx2 controls stereociliary bundle orientation of sensory hair cells. Nathans J, ed. *eLife*. 2017;6:e23661. https://doi.org/10.7554/eLife.23661
21. Crossley PH, Martin GR. The mouse Fgf8 gene encodes a family of polypeptides and is expressed in regions that direct outgrowth and patterning in the developing embryo. *Development*. 1995;121(2):439-451. https://doi.org/10.1242/dev.121.2.439
22. Dai J, Ma M, Niu Q, et al. Mastigoneme structure reveals insights into the O-linked glycosylation code of native hydroxyproline-rich helices. *Cell*. 2024;0(0). https://doi.org/10.1016/j.cell.2024.03.005
23. Das P, Mekonnen B, Alkhofash R, et al. The Small Interactor of PKD2 protein promotes the assembly and ciliary entry of the Chlamydomonas PKD2–mastigoneme complexes. *J Cell Sci*. 2024;137(1):jcs261497. https://doi.org/10.1242/jcs.261497
24. Liu P, Lou X, Wingfield JL, Lin J, Nicastro D, Lechtreck K. Chlamydomonas PKD2 organizes mastigonemes, hair-like glycoprotein polymers on cilia. *J Cell Biol*. 2020;219(6):e202001122. https://doi.org/10.1083/jcb.202001122
25. Yokoyama T, Copeland NG, Jenkins NA, Montgomery CA, Elder FFB, Overbeek PA. Reversal of Left-Right Asymmetry: a Situs Inversus Mutation. *Science*. 1993;260(5108):679-682. https://doi.org/10.1126/science.8480178
26. Bennett HW, Gustavsson AK, Bayas CA, et al. Novel fibrillar structure in the inversin compartment of primary cilia revealed by 3D single-molecule superresolution microscopy. *Mol Biol Cell*. 2020;31(7):619-639. https://doi.org/10.1091/mbc.E19-09-0499
27. Zhang XM, Ramalho-Santos M, McMahon AP. Smoothened Mutants Reveal Redundant Roles for Shh and Ihh Signaling Including Regulation of L/R Asymmetry by the Mouse Node. *Cell*. 2001;105(6):781-792. https://doi.org/10.1016/S0092-8674(01)00385-3
28. Vicidomini G, Moneron G, Han KY, et al. Sharper low-power STED nanoscopy by time gating. *Nat Methods*. 2011;8(7):571-573. https://doi.org/10.1038/nmeth.1624
29. Katoh TA, Omori T, Ishikawa T, Okada Y, Hamada H. Biophysical Analysis of Mechanical Signals in Immotile Cilia of Mouse Embryonic Nodes Using Advanced Microscopic Techniques. *Bio-Protoc*. 2023;13(14):e4715. https://doi.org/10.21769/BioProtoc.4715

30. Pomreinke AP, Soh GH, Rogers KW, Bergmann JK, Bläßle AJ, Müller P. Dynamics of BMP signaling and distribution during zebrafish dorsal-ventral patterning. Yelon D, ed. *eLife*. 2017;6:e25861. https://doi.org/10.7554/eLife.25861
31. Katoh TA, Ikegami K, Uchida N, et al. Three-dimensional tracking of microbeads attached to the tip of single isolated tracheal cilia beating under external load. *Sci Rep*. 2018;8(1):15562. https://doi.org/10.1038/s41598-018-33846-5
32. Djenoune L, Mahamdeh M, Truong TV, et al. Cilia function as calcium-mediated mechanosensors that instruct left-right asymmetry. *Science*. 2023;379(6627):71-78. https://doi.org/10.1126/science.abq7317
33. Oki S, Hashimoto R, Okui Y, et al. Sulfated glycosaminoglycans are necessary for Nodal signal transmission from the node to the left lateral plate in the mouse embryo. *Development*. 2007;134(21):3893-3904. https://doi.org/10.1242/dev.009464
34. Nakamura T, Mine N, Nakaguchi E, et al. Generation of Robust Left-Right Asymmetry in the Mouse Embryo Requires a Self-Enhancement and Lateral-Inhibition System. *Dev Cell*. 2006;11(4):495-504. https://doi.org/10.1016/j.devcel.2006.08.002
35. Berg HC, Purcell EM. Physics of chemoreception. *Biophys J*. 1977;20(2):193-219. https://doi.org/10.1016/S0006-3495(77)85544-6
36. Sulik K, Dehart DB, Inagaki T, et al. Morphogenesis of the murine node and notochordal plate. *Dev Dyn*. 1994;201(3):260-278. https://doi.org/10.1002/aja.1002010309
37. Lawson KA, Dunn NR, Roelen BAJ, et al. Bmp4 is required for the generation of primordial germ cells in the mouse embryo. *Genes Dev*. 1999;13(4):424-436.
38. Winnier G, Blessing M, Labosky PA, Hogan BL. Bone morphogenetic protein-4 is required for mesoderm formation and patterning in the mouse. *Genes Dev*. 1995;9(17):2105-2116. https://doi.org/10.1101/gad.9.17.2105
39. Krause C, Guzman A, Knaus P. Noggin. *Int J Biochem Cell Biol*. 2011;43(4):478-481. https://doi.org/10.1016/j.biocel.2011.01.007
40. Song K, Krause C, Shi S, et al. Identification of a Key Residue Mediating Bone Morphogenetic Protein (BMP)-6 Resistance to Noggin Inhibition Allows for Engineered BMPs with Superior Agonist Activity*. *J Biol Chem*. 2010;285(16):12169-12180. https://doi.org/10.1074/jbc.M109.087197
41. Kim RY, Robertson EJ, Solloway MJ. Bmp6 and Bmp7 Are Required for Cushion Formation and Septation in the Developing Mouse Heart. *Dev Biol*. 2001;235(2):449-466. https://doi.org/10.1006/dbio.2001.0284
42. Su X, Wu M, Yao G, et al. Regulation of polycystin-1 ciliary trafficking by motifs at its C-terminus and polycystin-2 but not by cleavage at the GPS site. *J Cell Sci*. 2015;128(22):4063-4073. https://doi.org/10.1242/jcs.160556
43. Oughtred R, Rust J, Chang C, et al. The BioGRID database: A comprehensive biomedical resource of curated protein, genetic, and chemical interactions. *Protein Sci*. 2021;30(1):187-200. https://doi.org/10.1002/pro.3978
44. Ishikawa H, Thompson J, Yates JR, Marshall WF. Proteomic Analysis of Mammalian Primary Cilia. *Curr Biol*. 2012;22(5):414-419. https://doi.org/10.1016/j.cub.2012.01.031
45. May EA, Kalocsay M, D'Auriac IG, et al. Time-resolved proteomics profiling of the ciliary Hedgehog response. *J Cell Biol*. 2021;220(5):e202007207. https://doi.org/10.1083/jcb.202007207
46. Mick DU, Rodrigues RB, Leib RD, et al. Proteomics of Primary Cilia by Proximity Labeling. *Dev Cell*. 2015;35(4):497-512. https://doi.org/10.1016/j.devcel.2015.10.015
47. Xie YF, Shi WG, Zhou J, et al. Pulsed electromagnetic fields stimulate osteogenic differentiation and maturation of osteoblasts by upregulating the expression of BMPRII

549 localized at the base of primary cilium. *Bone*. 2016;93:22-32.
550 https://doi.org/10.1016/j.bone.2016.09.008
551 48. Field S, Riley KL, Grimes DT, et al. Pkd1l1 establishes left-right asymmetry and
552 physically interacts with Pkd2. *Development*. 2011;138(6):1131-1142.
553 https://doi.org/10.1242/dev.058149
554 49. Grimes DT, Keynton JL, Buenavista MT, et al. Genetic Analysis Reveals a Hierarchy
555 of Interactions between Polycystin-Encoding Genes and Genes Controlling Cilia Function
556 during Left-Right Determination. *PLOS Genet*. 2016;12(6):e1006070.
557 https://doi.org/10.1371/journal.pgen.1006070
558 50. Katoh TA, Fukai YT, Ishibashi T. Optical microscopic imaging, manipulation, and
559 analysis methods for morphogenesis research. *Microscopy*. Published online December 15,
560 2023:dfad059. https://doi.org/10.1093/jmicro/dfad059
561 51. Weiss LE, Milenkovic L, Yoon J, Stearns T, Moerner WE. Motional dynamics of
562 single Patched1 molecules in cilia are controlled by Hedgehog and cholesterol. *Proc Natl*
563 *Acad Sci*. 2019;116(12):5550-5557. https://doi.org/10.1073/pnas.1816747116
564
565

Figure Legends

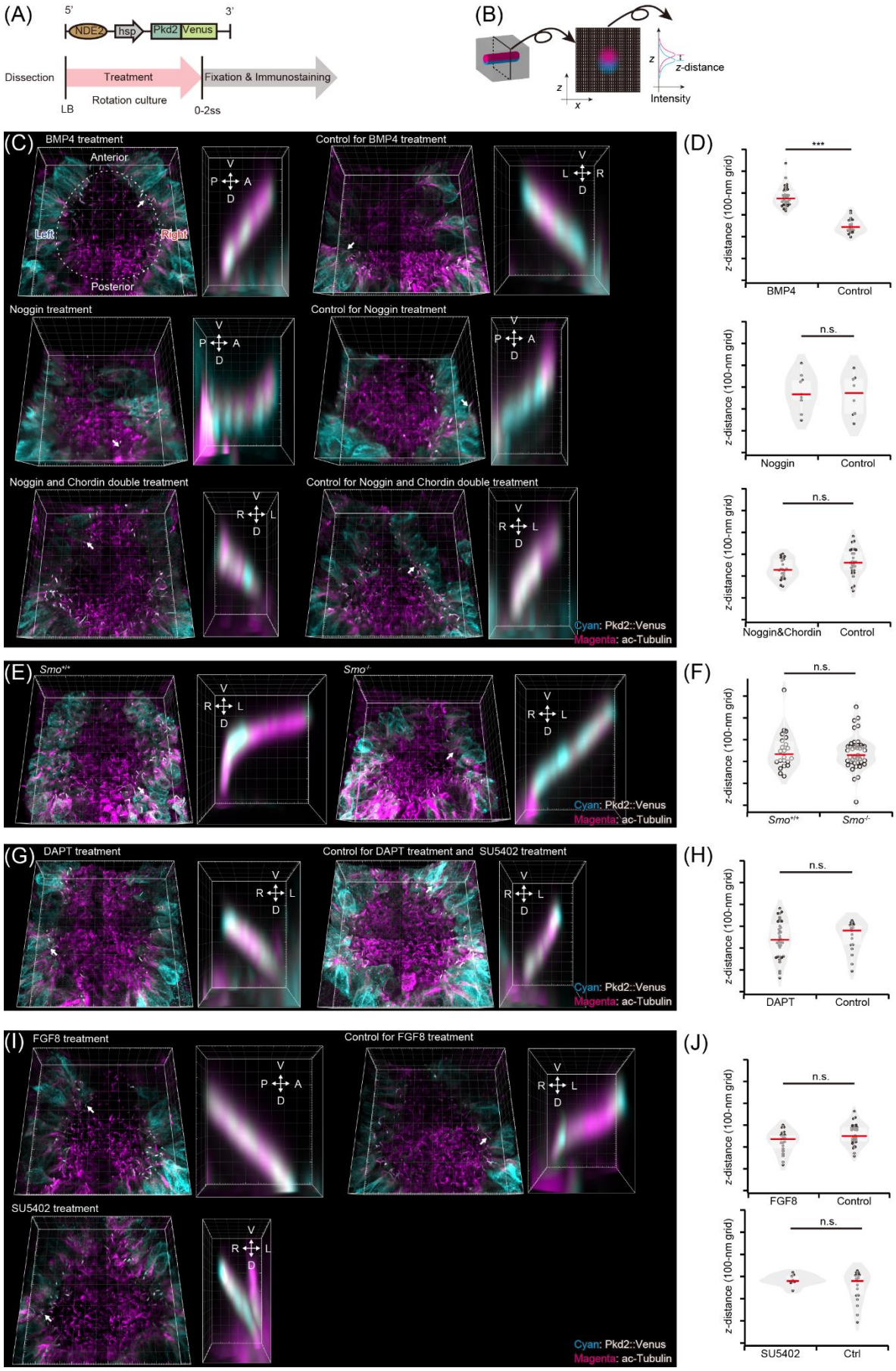

Figure 1. Pkd2 distribution in immotile cilia in the presence of various recombinant proteins and inhibitors and mutant embryos.

(A) Wild-type mouse embryo harboring the *NDE2-hsp-Pkd2-Venus* transgene was cultured in agent-containing medium from the late bud (LB) stage to 0–2 somite stages (ss). The embryos were fixed with paraformaldehyde and immunostained with the Pkd2::Venus fusion protein and acetylated tubulin. Nodal immotile cilia were observed using a confocal microscope equipped with an Airyscan detector and 100× objective. **(B)** Distance between the centers of the red and green channels along the *z*-axis was measured via one-dimensional Gaussian fitting (illustrated in magenta and cyan, respectively). **(C, E, G, I)** Immunofluorescence analysis to detect the Pkd2::Venus fusion protein (cyan) and acetylated (ac) tubulin (magenta) at the node using an Airyscan microscope. Magnified images of the dorsoventral (D–V) sections of nodal immotile cilia, indicated by white arrows, are shown on the right. Grid size, 5 and 0.5 μm for the main and magnified panels, respectively. **(C)** Effect of the bone morphogenetic protein 4 (BMP4) signal on the Pkd2 distribution. Images of embryos cultured in a 1 μg/mL BMP4-containing medium (left top image), 1 μg/mL Noggin-containing medium (left middle image), 1 μg/mL Noggin- and 1 μg/mL Chordin-containing medium (left bottom image), and under control conditions (right images). **(D)** Distance along the *z*-axis between the red and green channels in BMP4-treated embryos was larger (133 ± 122 nm) than that in control embryos (n = 32 and 19 cilia for BMP4-treatment and control, respectively; upper panel). Distance along the *z*-axis between the red and green channels in Noggin-treated embryos was slightly smaller (15 ± 316 nm) than that in control embryos, but the difference in distribution was not significant (n = 26 and 12 cilia for Noggin-treatment and the control, respectively; middle panel). Distance along the *z*-axis between the red and green channels in Noggin and Chordin double-treated embryos was slightly smaller (31 ± 107 nm) than that in control embryos, but the difference was not significant (n = 22 and 27 cilia for Noggin and Chordin double-treatment and control, respectively; lower panel). **(E)** Effect of the sonic hedgehog (SHH) signal on Pkd2 distribution. Images of *Smo*$^{-/-}$ (left images) and control (right images) embryos. **(F)** Distance along the *z*-axis between the red and green channels in *Smo*$^{-/-}$ embryos was slightly smaller (9 ± 205 nm) than that in control embryos, but the difference in distribution was not significant (n = 43 and 22 cilia for *Smo*$^{-/-}$ and control embryos, respectively). **(G)** Effect of the Notch signal on Pkd2 distribution. Images of embryos cultured in a 200 μM *N*-[*N*-(3, 5-difluorophenacetyl)-l-alanyl]-*S*-phenylglycine *t*-butyl ester (DAPT)-containing medium (left images) and under control conditions (right images). **(H)** Distance along the *z*-axis between the red and green channels in DAPT-treated embryos was slightly smaller (11 ± 170 nm) than that in the control embryos, but the difference in distribution was not significant (n = 36 and 17 cilia for DAPT-treatment and control, respectively). **(I)** Effect of the fibroblast growth factor (FGF) signal on the Pkd2 distribution. Images of embryos cultured in a 1 μg/mL FGF-8b-containing medium (left upper images), 25 μM SU5402-containing medium (left upper images), and under control conditions (right images). **(J)** Distance along the *z*-axis between the red and green channels in FGF-

8b-treated embryos was slightly smaller (32 ± 40 nm) than that in the control embryos, but the difference in distribution was not significant (n = 21 and 30 cilia for FGF-8b treatment and control, respectively). Distance along the z-axis between the red and green channels in SU5402-treated embryos was larger (70 ± 147 nm) than that in the control embryos (same data as the control for DAPT-treatment), but the difference in distribution was not significant (n = 17 cilia for SU5402 treatment). **(H, J)** Note that the control for DAPT treatment and SU5402 treatment is the same dataset. **(D, F, H, J)** Red bars indicate the median values. ***P < 0.001; n.s., not significant (Mann–Whitney U test).

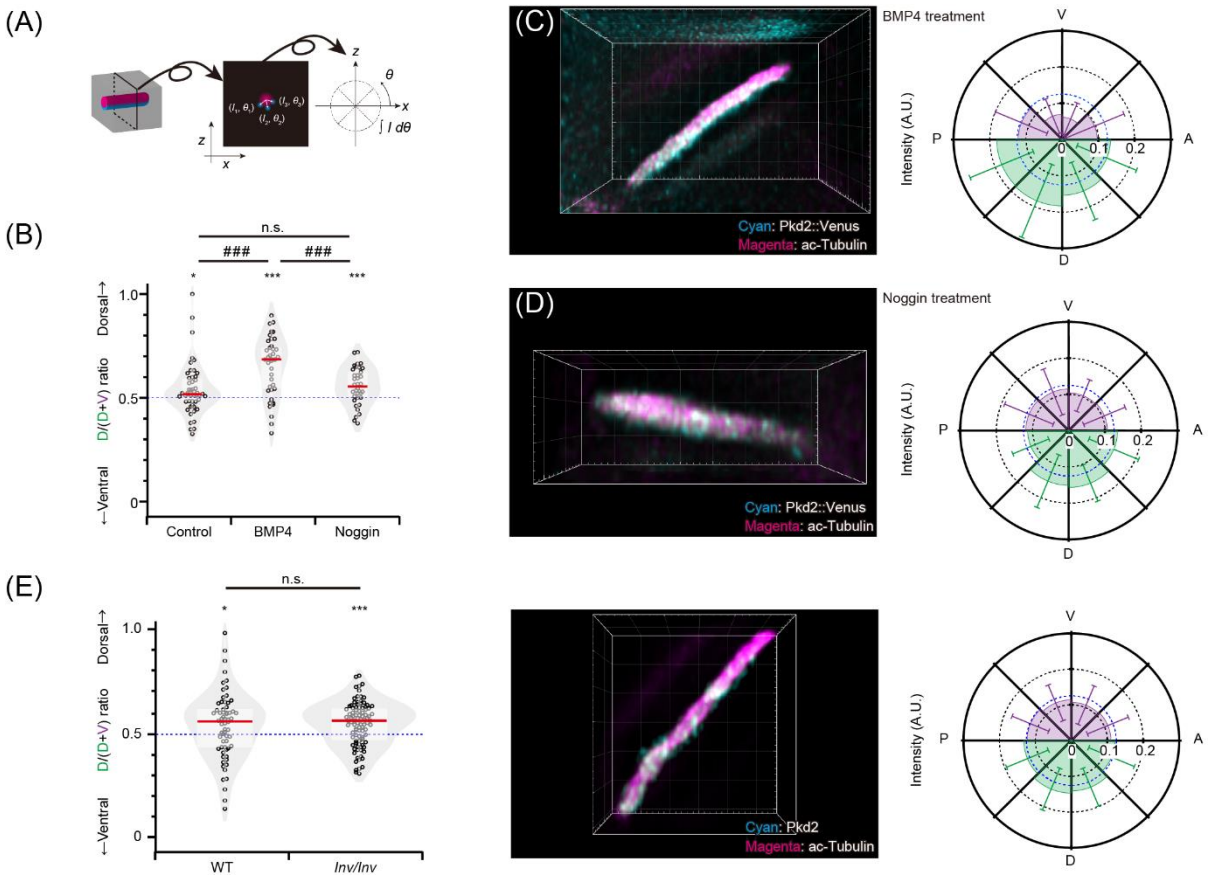

Figure 2. Angular distribution of Pkd2 in the presence of recombinant BMP4 or Noggin protein evaluated using 3D-stimulated emission depletion (STED) microscope.

(A) Wild-type mouse embryos harboring the *NDE2-hsp-Pkd2-Venus* transgene were cultured in agent-containing medium from LB to 0–2 ss. The embryos were immunostained with anti-green fluorescent protein (green channel; illustrated in cyan) and anti-acetylated tubulin (red channel; illustrated in magenta) and observed using 3D-STED microscopy. Green fluorescence intensity in transverse planes of each cilium was analyzed and plotted with each 45° sector based on the gravity center of red fluorescence intensity. **(B)** Ratio of Pkd2::Venus signal intensity on the dorsal side to that on the dorsal plus ventral sides (D / [D + V]). Ratio in the cilia of BMP4-treated embryos was significantly larger than that in the cilia of previously reported wild-type embryos[5] and Noggin-treated embryos. Interestingly, the ratio in the cilia of Noggin-treated embryos did not significantly differ compared with that of previously reported wild-type embryos.[5] Red bars indicate the median values. **P* < 0.05; ****P* < 0.001 (one-sample *t* test). ###*P* < 0.001; n.s., not significant (Mann–Whitney *U* test). **(C, D)** Immunofluorescence analysis to detect the Pkd2::Venus fusion protein (cyan) and acetylated (ac) tubulin (magenta) at the node using a 3D-STED microscope after BMP4 (C) or Noggin (D) treatment. Grid size, 500 nm. **(C)** Magnified views of D–V sections of BMP4-treated cilia observed using the 3D-STED microscope (left). Angular distribution of green fluorescence intensity in the transverse planes of BMP4-treated cilia was analyzed (*n* = 40 cilia; right). **(D)** Magnified views of D–V sections of Noggin-treated cilium observed using the 3D-STED microscope (left). Angular

distribution of green fluorescence intensity in the transverse planes of Noggin-treated cilia was analyzed (n = 36 cilia; right). **(E)** Ratio of Pkd2 signal intensity on the dorsal side to that on the dorsal plus ventral sides (D / [D + V]). Ratio of the signal intensity in the cilia of *Inv/Inv* embryos was comparable to that of previously reported wild-type embryos.[5] Red bars indicate the median values. *P < 0.05; ***P < 0.001 (one-sample t test). ###P < 0.001; n.s., not significant (Mann–Whitney U test). Grid size, 500 nm.

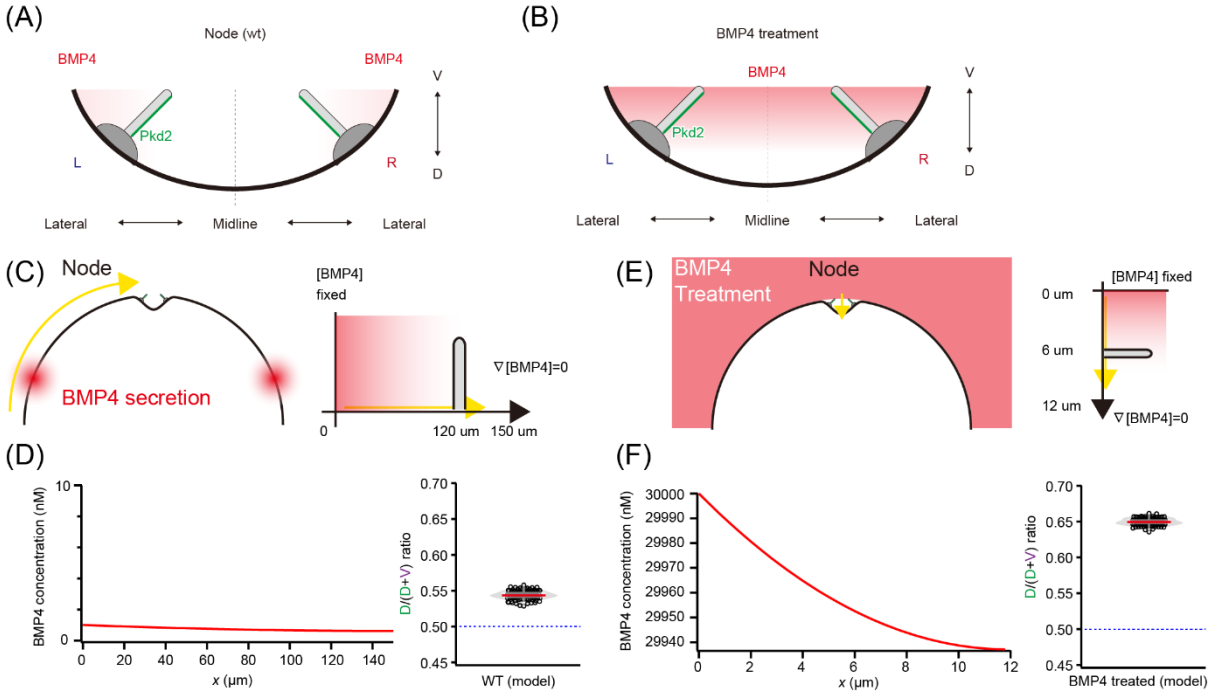

Figure 3. Calculation of BMP4 concentration and model of regulation of asymmetric Pkd2 distribution.

(A) BMP4 is expressed in the lateral plate mesoderm (LPM). Endogenous expression of BMP4 generates a concentration gradient from the LPM to the node. The asymmetric distribution may be explained by this BMP4 gradient, which enables the arrangement of Pkd2 molecules away from the high BMP4 concentration regions. **(B)** In the presence of excess BMP4, the BMP4 gradient may be increased locoregionally, causing more asymmetric Pkd2 distribution and enrichment in the dorsal region. **(C)** Schematic of the model of the wild-type (WT) embryo. BMP4 was secreted from the LPM (depicted as a red sphere), with the left side of the LPM defined as x = 0 μm. The center of the node was positioned 150 μm from the left side of LPM, and immotile cilia on the left side were 120 μm from the left side of LPM. BMP4 concentration was maintained at 1 nM on the left side of LPM, and BMP4 diffused from this point. **(D)** Calculated BMP4 concentration along the left side of LPM to the node in the WT embryo (left). The concentration at 5000 s, after reaching a plateau, is shown. The resulting Pkd2 distribution in cilia is shown as the D/(D + V) ratio (right). **(E)** Schematic of the model of BMP4 treatment. The medium contained a high concentration of BMP4 (depicted in red). Upper side of the node was defined as x = 0 μm, and the node depth was defined as 12 μm. Immotile cilia were 6 μm from the bottom of the node. BMP4 concentration in the medium was maintained at 30 μM, and BMP4 diffused into the node. **(F)** Calculated BMP4 concentration from the upper to the bottom of the node under BMP4 treatment (left). The concentration at 3600 s, after reaching a plateau, is shown. The resulting Pkd2 distribution in cilia is shown as the D/(D + V) ratio (right).

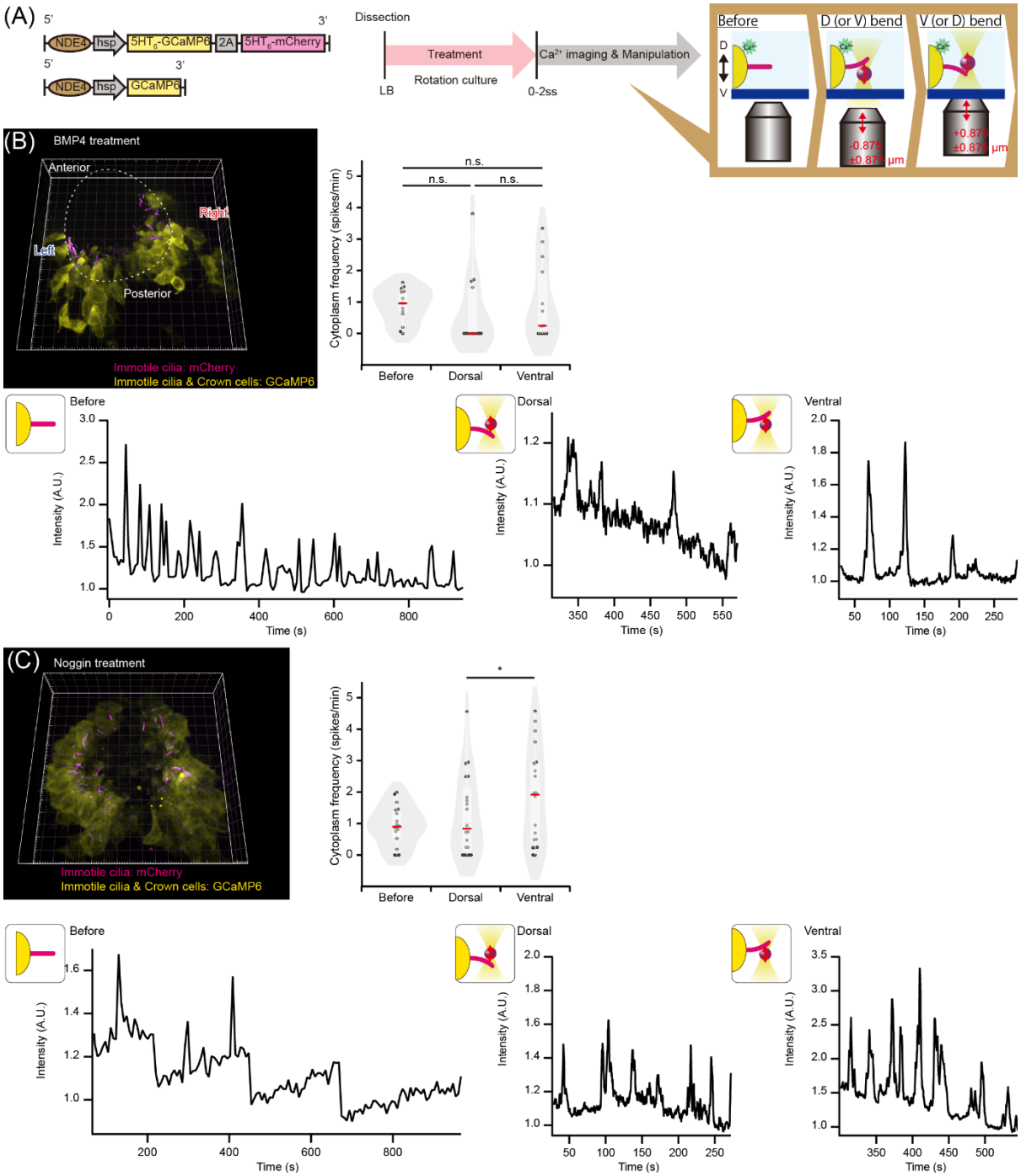

Figure 4. Calcium response in crown cells triggered by mechanical stimuli to the cilium in the presence of recombinant BMP4 or Noggin protein.

(A) Experiments were performed using *iv/iv* mouse embryos harboring two transgenes. Immotile cilia at the node were visualized based on mCherry expression, which is regulated by a nodal-specific enhancer (NDE) and targeted to cilia by a 5-hydroxytryptamine receptor isoform 6 ($5HT_6$) sequence (upper left). GCaMP6 was expressed in the cytoplasm for cytoplasmic calcium imaging (lower left). The embryos were cultured in agent-containing medium from LB to 0–2 ss and subjected to calcium imaging (middle panel). The cilium was subjected to sequential dorsal and ventral bending by a polystyrene bead trapped using optical tweezers. A bead was trapped, displaced to z = –1.75 µm

(equivalent to the radius of the bead; the minus sign indicates the ventral direction according to the use of an inverted microscope), and made to contact the ventral side of the cilium. The cilium was subjected to dorsal bending of –0.875 μm at 2 Hz with an amplitude of ±0.875 μm for approximately 250 s (cilium was bent 0 to 1.75 μm toward the dorsal side; middle in the right panel) and then bent ventrally at +0.875 μm at 2 Hz with an amplitude of ±0.875 μm for approximately 250 s (right in the right panel). **(B)** Three-dimensional image of the node of a BMP4-treated embryo (left top). Grid size, 10 μm. The mean frequency of the calcium transient in the cytoplasm before stimulation, during dorsal bending, and during ventral bending (*n* = 13 cilia; right top). Average ± standard deviation (SD) values of the mean calcium frequency were 0.89 ± 0.53, 0.66 ± 1.13, and 0.98 ± 1.19 Hz before stimulation, during dorsal bending, and during ventral bending, respectively. Red bars indicate the median values. Time course of cytoplasmic calcium signal intensity in the crown cell before stimulation (left bottom), during dorsal bending (middle bottom), and during ventral bending (right bottom) (GCaMP6 F/F_0 ratiometric values). **(C)** Three-dimensional image of the node of Noggin-treated embryos (left top). Grid size, 10 μm. The mean frequency of calcium transient in the cytoplasm before stimulation, during dorsal bending, and during ventral bending (*n* = 18, 20, and 20 cilia for before stimulation, during dorsal bending, and during ventral bending, respectively; right top). Average ± SD values of the mean calcium frequency were 0.93 ± 0.61, 1.27 ± 1.25, and 1.83 ± 1.49 Hz before stimulation, during dorsal bending, and during ventral bending, respectively. Red bars indicate the median values. Time course of cytoplasmic calcium signal intensity in the crown cells before stimulation (left bottom), during dorsal bending (middle bottom), and during ventral bending (right bottom; GCaMP6 F/F_0 ratiometric values).

Table

Table 1. Model parameters (see Figure 4)

		Wild-type	BMP4 treatment
Parameters for calculating BMP4 diffusion	Diffusion constant of BMP4 (D_b; use value for BMP2b[30])	3 μm^2/s	3 μm^2/s
	Initial concentration of BMP4 at the center of the node	0 M	0 M
	BMP4 concentration in LPM	1 nM	-
	BMP4 concentration in the medium	-	30 μM (1 μg/mL)
	Degradation constant of BMP4 (λ; use value for BMP2b[30])	8.9×10^{-5} /s	8.9×10^{-5} /s
	Duration	5000 s	3600 s
Parameters for modeling the asymmetric Pkd2 distribution in cilia	Diffusion constant of Pkd2 in cilia (value for PTCH1[51])	0.1 μm^2/s	0.1 μm^2/s
	Sensitivity of BMP4 concentration gradient for Pkd2 distribution regulation (S)	8×10^{10}	6×10^{7}
	Estimated D/(D + V) ratio of Pkd2 (see Figure 4D,F)	0.54 ± 0.01	0.65 ± 0.01

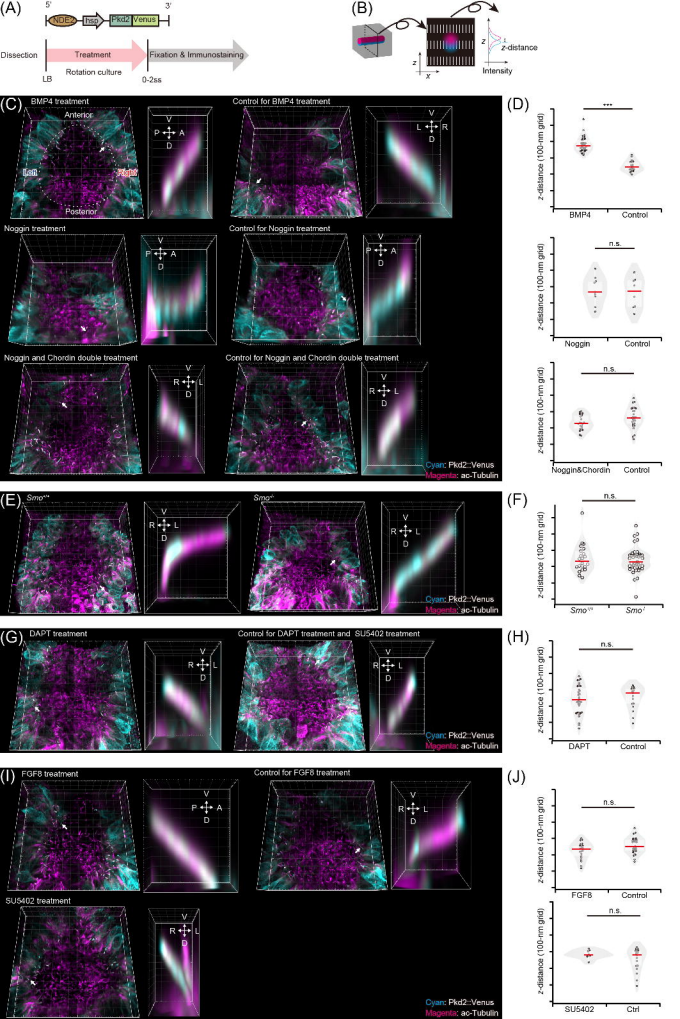
(A)
5'
hCEC
Hes1
Pkd2
Venus
3'
Dissection
Treatment
Fixation & Immunostaining
LB
Rotation culture
0-2ss
(B)
z
x
z-distance
Intensity
(C)
BMP4 treatment
Anterior
Posterior
Left
Right
Control for BMP4 treatment
Noggin treatment
Control for Noggin treatment
Noggin and Chordin double treatment
Control for Noggin and Chordin double treatment
Cyan: Pkd2::Venus
Magenta: ac-Tubulin
(D)
***
n.s.
z-distance (100-nm grid)
BMP4
Control
Noggin
Noggin&Chordin
(E)
Smo-/-
Smo+/+
(F)
Smo-/-
Smo+/+
(G)
DAPT treatment
Control for DAPT treatment and SU5402 treatment
(H)
DAPT
Control
(I)
FGF8 treatment
Control for FGF8 treatment
SU5402 treatment
(J)
FGF8
Control
SU5402
Ctrl

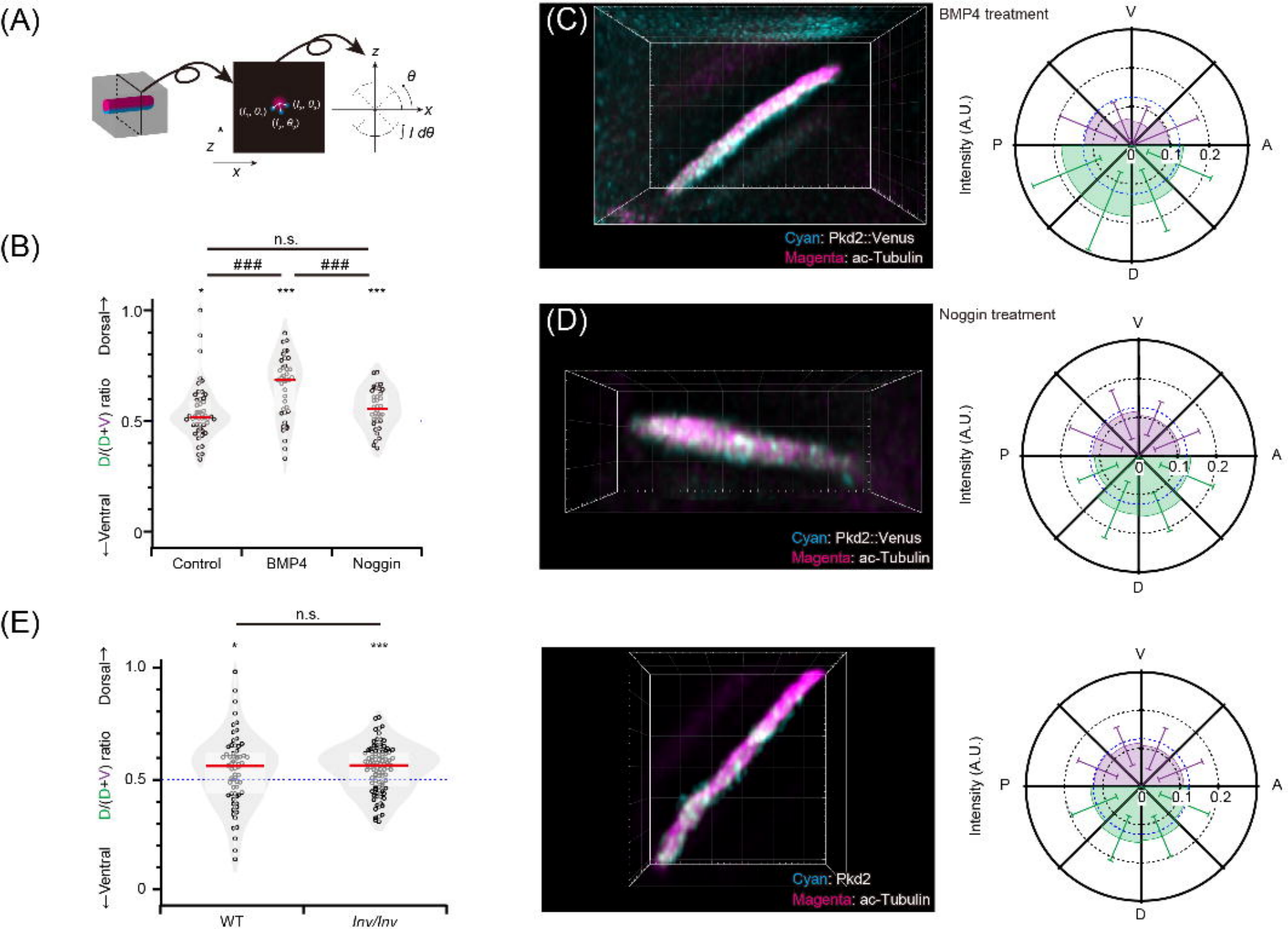
(A)
z
θ
x
∫ I dθ
z
x
(B)
n.s.
###
###
***
***
1.0
0.5
0
Dorsal→
D/(D+V) ratio
←Ventral
Control
BMP4
Noggin
(C)
Cyan: Pkd2::Venus
Magenta: ac-Tubulin
BMP4 treatment
V
P
A
D
Intensity (A.U.)
0
0.1
0.2
(D)
Cyan: Pkd2::Venus
Magenta: ac-Tubulin
Noggin treatment
V
P
A
D
Intensity (A.U.)
0
0.1
0.2
(E)
n.s.
*
***
1.0
0.5
0
Dorsal→
D/(D+V) ratio
←Ventral
WT
Inv/Inv
Cyan: Pkd2
Magenta: ac-Tubulin
V
P
A
D
Intensity (A.U.)
0
0.1
0.2

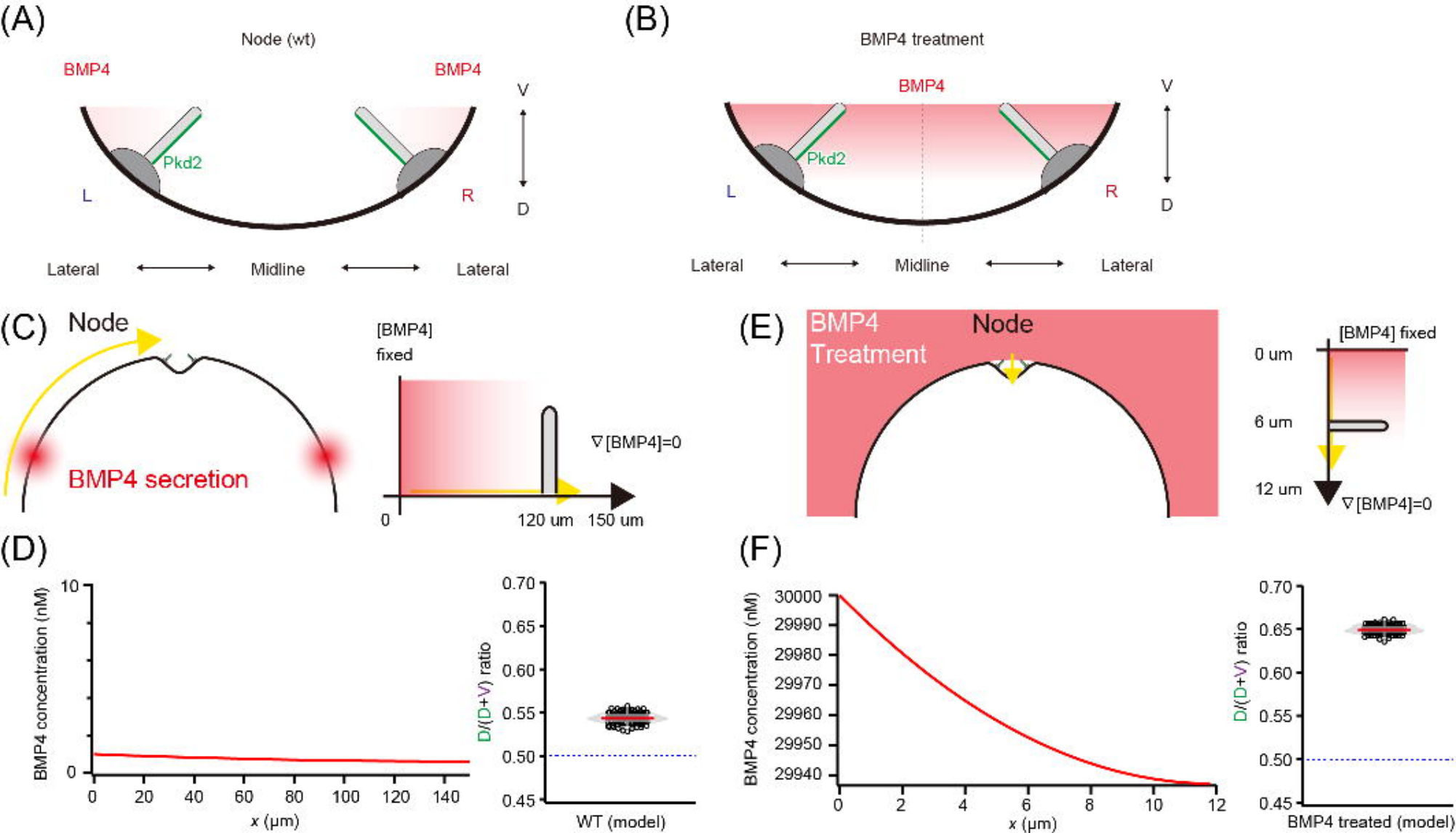
(A)
Node (wt)
BMP4
BMP4
Pkd2
L
R
V
D
Lateral
Midline
Lateral
(B)
BMP4 treatment
BMP4
Pkd2
L
R
V
D
Lateral
Midline
Lateral
(C)
Node
BMP4 secretion
[BMP4]
fixed
∇[BMP4]=0
0
120 um
150 um
(E)
BMP4
Treatment
Node
[BMP4] fixed
0 um
6 um
12 um
∇[BMP4]=0
(D)
BMP4 concentration (nM)
10
0
0
20
40
60
80
100
120
140
x (μm)
D/(D+V) ratio
0.70
0.65
0.60
0.55
0.50
0.45
WT (model)
(F)
BMP4 concentration (nM)
30000
29990
29980
29970
29960
29950
29940
0
2
4
6
8
10
12
x (μm)
D/(D+V) ratio
0.70
0.65
0.60
0.55
0.50
0.45
BMP4 treated (model)

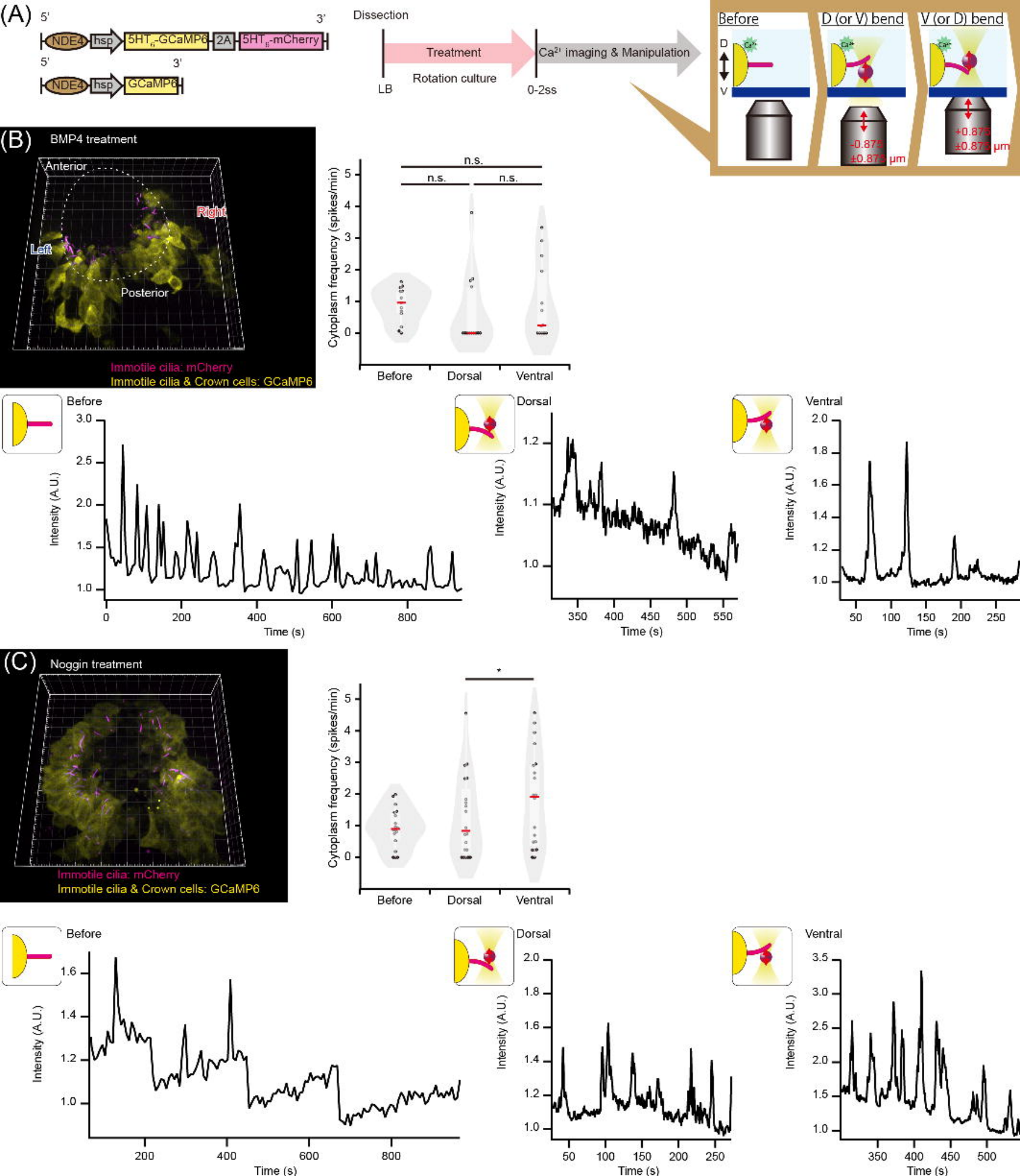
(A)
5'
3'
NDE4
hsp
5HT1A-GCaMP6
2A
5HT1B-mCherry
5'
3'
NDE4
hsp
GCaMP6
Dissection
Treatment
Rotation culture
LB
Ca2+ imaging & Manipulation
0-2ss
Before
D (or V) bend
V (or D) bend
D
V
-0.875 ±0.875 μm
+0.875 ±0.875 μm
(B)
BMP4 treatment
Anterior
Right
Left
Posterior
Immotile cilia: mCherry
Immotile cilia & Crown cells: GCaMP6
n.s.
n.s.
n.s.
Cytoplasm frequency (spikes/min)
Before
Dorsal
Ventral
Before
Intensity (A.U.)
Time (s)
Dorsal
Intensity (A.U.)
Time (s)
Ventral
Intensity (A.U.)
Time (s)
(C)
Noggin treatment
Immotile cilia: mCherry
Immotile cilia & Crown cells: GCaMP6
*
Cytoplasm frequency (spikes/min)
Before
Dorsal
Ventral
Before
Intensity (A.U.)
Time (s)
Dorsal
Intensity (A.U.)
Time (s)
Ventral
Intensity (A.U.)
Time (s)